AGARD 52nd Specialists' Meeting of the Electromagnetic Wave Propagation Panel
Palma De Mallorca, Spain, 17-21 May 1993

CONFERENCE HANDOUT

PROPAGATION MODELING OF MOIST AIR AND SUSPENDED WATER/ICE PARTICLES AT FREQUENCIES BELOW 1000 GHz

H. J. Liebe
G. A. Hufford
M. G. Cotton
National Telecommunications and Information Administration
Institute for Telecommunication Sciences
325 Broadway, Boulder, CO 80303
U.S.A

SUMMARY

Propagation characteristics of the atmosphere are modeled for frequencies up to 1000 GHz by the Millimeter-wave Propagation Model MPM. In three routines MPM computes the absorption and delay spectra of main natural absorbers (i.e., oxygen, water-vapor, suspended droplets and ice particles) from known meteorological variables. The *dry-air* module deals with contributions from 44 local lines and is supported by extensive 60-GHz laboratory absorption measurements of the pressure-broadened O_2 spectrum. The *water-vapor* module considers 34 local H_2O lines and continuum contributions from the rotational H_2O spectrum above 1 THz. The continuum is formulated as low-frequency wing response of a pseudo-line centered at 1.8 THz. The *suspended-particle* module employs revised formulations for the permittivities of water and ice and the Rayleigh absorption approximation.

At altitudes between 30 and 120 km, the Earth's geomagnetic field influences the oxygen absorption lines. The resulting anisotropic medium properties are computed by the Zeeman Propagation Model ZPM. The elements of a refractivity tensor are determined in the vicinity ($\pm$10 MHz) of O_2 microwave lines and their effect on the propagation of a plane, polarized wave is evaluated.

A spherically stratified (0 - 130 km) atmosphere with height profiles for air density, water vapor mixing ratio, and the geomagnetic field provides the geometry for analyzing geocoded transmission and emission characteristics. Polarization-sensitive and direction-dependent propagation is predicted through the mesosphere. More specifically, high-resolution emission spectra of the 9^+ line (61150 $\pm$ 3 MHz) for paths looking from space through the atmosphere with tangential heights ranging from 30 to 125 km are consistent with recent observations.

1. INTRODUCTION

The natural atmospheric absorbers of oxygen, water vapor, and suspended water-droplets or ice-crystals, determine the propagation properties of the nonprecipitating atmosphere. The spectral characteristics of these absorbers are predicted up to 1000 GHz based on the physical conditions at altitudes from sea level to 130 km. Both phase and amplitude response of a plane radio wave propagating the distance z at frequency ν are described by a field strength,

$$E(z) = \exp[\, i\, k\, z(\, 1 + N\times 10^{-6}\,)]\, E(0),$$

where E(0) is the initial value, $k = 2\pi\nu/c$ is the free space wave number, and c is the speed of light in vacuum. The spectral characteristics of the atmospheric medium are expressed by a complex refractivity,

$$N = N_o + N' + i\, N'' \quad \text{ppm} \qquad (1)$$

The real part changes the propagation velocity (refraction) and consists of a frequency-independent term, N_o, plus the dispersive refraction $N'(\nu)$. The imaginary part quantifies the loss of radiation energy (absorption). Refractivity N determines the specific quantities of power attenuation α and phase dispersion β or delay rate τ. Assuming frequency ν in GHz one obtains:

$$\alpha = 0.1820\, \nu\, N'' \quad \text{dB/km},$$
$$\beta = 1.2008\, \nu\, (N_o + N') \quad \text{deg/km},$$
$$\tau = 3.3356\, (N_o + N') \quad \text{ps/km}.$$

Under special circumstances the refractivity N can exhibit *anisotropic* properties (e.g., mesospheric O_2 Zeeman effect). In such a case the propagation of plane, polarized waves is characterized by a two-dimensional field vector $\mathbf{E}^*(z)$ which is affected perpendicular to the direction of propagation by a 2×2 refractivity matrix $\mathbf{N}$.

2. ATMOSPHERIC REFRACTIVITY

2.1 Input Variables

Complex refractivity N is the central quantity computed by the Millimeter-wave Propagation Model MPM.[1,2] Here, the opportunity is taken to update MPM89 [2] with the latest spectroscopic information. The model considers 44 O_2 and 34 H_2O local lines (centered below 1000 GHz), nonresonant spectra for dry air, and an empirical water vapor continuum which reconciles experimental discrepancies. Model formulations for dry air and water vapor spectra follow closely the theory of absorption by atmospheric gases that is reviewed in detail by Rosenkranz.[3] The refractivity of suspended water and ice particles is computed with the Rayleigh absorption approximation.[4] The nomenclature and limits for atmospheric physical conditions are as follows.

		Typical Range:	
- barometric pressure	p	10^{-5} - 1013	mb
- ambient temperature	t	-100 - 50	°C
- relative humidity	u	1 - 100	%
- water droplet density	w	0 - 5	g/m^3
- ice particle density	w_i	0 - 1	g/m^3

For modeling purposes, a reciprocal temperature variable is introduced, $\theta = 300/(t + 273.15)$, and the barometric pressure p (1 mb = 100 Pa) is separated into partial pressures for dry air (p_d) and water vapor (e); i.e.,

$$p = p_d + e \quad \text{mb}.$$

2.2 Oxygen Spectrum

2.2.1 *Pressure-Broadening*

Refractivity of molecular oxygen in dry air is expressed by

$$N_D = N_d + \Sigma_k S_k F_k + N_n \quad \text{ppm}, \qquad (2)$$

where the nondispersive term is

$$N_d = 0.2588\, p_d\, \theta\,.$$

The main contributions come from 44 O_2 spectral lines (k = line index). Each line strength,

$$S_k = (a_1 / \nu_k)\, p_d\, \theta^3 \exp[a_2 (1 - \theta)] \quad \text{ppm},$$

is multiplied by the complex shape function,

$$F(\nu) = \nu \left[\frac{1 - i\delta_k}{\nu_k - \nu - i\gamma_k} - \frac{1 + i\delta_k}{\nu_k + \nu + i\gamma_k} \right] \qquad (3)$$

The Van Vleck-Weisskopf function $F(\nu)$ was modified by Rosenkranz [3] to include line overlap effects. Width (γ) and overlap (δ) parameters of pressure-broadened O_2 lines in air are

$$\gamma_k = a_3 \times 10^{-3} (p_d\, \theta^{a4} + 1.10\, e\, \theta) \quad \text{GHz}$$

and

$$\delta_k = (a_5 + a_6\, \theta)\, p\, \theta^{0.8}.$$

Extensive laboratory measurements of 60-GHz absorption by dry air have been reported recently.[5] A best fit to these data established new coefficients a_5 and a_6 for the microwave lines. Still, the values listed for a_3 and $a_{5,6}$ in Table 1 are different from Ref. 5: indirect evidence from the data suggests that all microwave widths γ_k are multiplied by 1.05. This correction reduced on the average by 7 percent the rms error of the residuals for all 5400 data points when, in addition, the δ_k's were raised by a factor of 1.15. [5] Center frequencies ν_k and spectroscopic coefficients a_1 to a_6 are listed in Table 1.

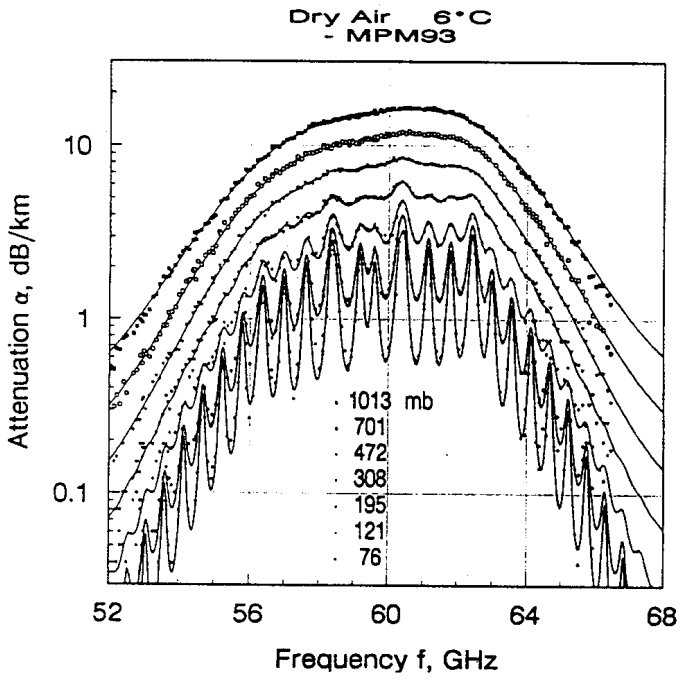

Figure 1. Dry air attenuation α from 52 to 68 GHz at 6°C for pressures from 1013 to 76 mb: MPM93 (lines), measured data [5] (symbols).

An example of predicted attenuation rates and measured data points is shown in Fig. 1. Some of the very first attenuation rates (14 values, 49 - 59 GHz) for sea-level conditions were reported in 1956. [6] These field-measured data agree well with predictions based on Eq. (2).

2.2.2 *Nonresonant Terms*

Nonresonant refractivity is given by,

$$N_n = S_o F_o(\nu) + i\, S_n F_n''(\nu) \quad \text{ppm}.$$

The O_2 relaxation spectrum is computed by means of

$$S_o = 6.14 \times 10^{-5}\, p_d\, \theta^2,$$

$$F_o = -\nu / (\nu + i\, \gamma_o),$$

where the relaxation frequency is $\gamma_o = 0.56 \times 10^{-3}\, p\, \theta^{0.8}$. In addition, pressure-induced N_2 absorption,

$$S_n = 1.40 \times 10^{-12}\, p_d^2\, \theta^{3.5},$$

$$F_n'' \approx \nu / (1 + 1.9 \times 10^{-5}\, \nu^{1.5}),$$

makes a small contribution to N_D above 100 GHz.

2.2.3 *Zeeman-Broadening*

In the mesosphere, oxygen line absorption is complicated.[7] Three separate complex-valued Zeeman refractivity patterns, $N_{\sigma\pm}$ and N_π, are brought out by the geomagnetic field vector $\mathbf{B}$. The refractivity that influences the field components of a plane wave is expressed in matrix form, [8]

$$N = \begin{vmatrix} N_\pi \sin^2\phi + (N_{\sigma+} + N_{\sigma-})\cos^2\phi & -i\,(N_{\sigma+} - N_{\sigma-})\cos\phi \\ i\,(N_{\sigma+} + N_{\sigma-})\cos\phi & N_{\sigma+} + N_{\sigma-} \end{vmatrix}$$

where ϕ is the angle between the direction of propagation and the magnetic vector $\mathbf{B}$. The Zeeman refractivities of one isolated line are represented by

$$N_{\sigma\pm,\pi} = N_d + S_k \Sigma_M \xi_M F_M \quad \text{ppm}, \qquad (4)$$

where ξ_M is a relative strength factor defined in such a way that the sum of the Zeeman components equals the strength value (a_1) of the unsplit (B = 0) line. The center frequency of individual lines within a pattern is determined by

$$\nu_M = \nu_k + 28.03 \times 10^{-6}\, \eta_M\, B \quad \text{GHz},$$

where the relative shift factor η_M lies between + 1 and - 1. The index M stands for the azimuthal quantum number M, which controls the structure of a Zeeman pattern.[9] The scheme for determining ξ_M and η_M hinges on the quantum number identification of a particular O_2 line and can be found in Refs. 8, 9. The shape function is approximated by a single Lorentzian,

$$F_M = \nu / (\nu_M - \nu - i\, \gamma_h),$$

and will be replaced by a Voigt profile.[3] The transition to Doppler-broadening at pressures $p \le 0.8$ mb ($h \ge 50$ km) is approximated for each Zeeman component by the width

$$\gamma_h = 0.535\, \gamma_k + (0.217\, \gamma_k^2 + \gamma_D^2)^{1/2} \quad \text{GHz},$$

where the Doppler width is $\gamma_D = 1.096 \times 10^{-6}\, \nu_M\, \theta^{-1/2}$. A rough estimate of line behavior in the mesosphere can be obtained by replacing γ_k with

$$\gamma_h = (\gamma_k^2 + 625\, B^2)^{1/2},$$

where B is the magnetic field strength (22 - 65 μT) depending on the geographic location and altitude.

2.3 Water Vapor Spectrum

The MPM-input for water vapor is relative humidity u, which is converted to vapor pressure $e = (u/100)\, e_S$ by way of the saturation pressure e_S over water (or ice) [10] at temperature t. A useful approximation for saturation over water is given by

$$e_S = 2.408\times10^{11}\,\theta^5 \exp(-22.644\,\theta) \quad \text{mb}.$$

Absolute humidity (vapor density) follows from

$$q = 0.7223\, e\,\theta \quad \text{g/m}^3.$$

Refractivity of atmospheric water vapor is written in the form

$$N_V = N_v + \sum_\ell S_\ell F_\ell + N_c \quad \text{ppm}, \qquad (5)$$

where the nondispersive term is

$$N_v = (4.163\,\theta + 0.239)\, e\,\theta\,.$$

Line refractivity results from 34 local H_2O resonances (ℓ = line index). The line strength is

$$S_\ell = (b_1/\nu_\ell)\, e\,\theta^{3.5} \exp[b_2(1-\theta)] \quad \text{ppm},$$

the shape function is formulated by Eq. (3). The width of a pressure-broadened H_2O line is formulated by [11]

$$\gamma_\ell = b_3\times10^{-3}\,(b_4\, e\,\theta^{b6} + p_d\,\theta^{b5}) \quad \text{GHz}.$$

Line overlap is neglected ($\delta_\ell = 0$) and Doppler-broadening is approximated for pressures below 0.7 mb ($h \geq 60$ km) by

$$\gamma_\ell^* = 0.535\,\gamma_\ell + (0.217\,\gamma_\ell^2 + \gamma_D^2)^{1/2},$$

where the Doppler width is $\gamma_D = 1.46\times10^{-6}\,\nu_\ell\,\theta^{-1/2}$.

2.3.2 *Water Vapor Continuum*

The contributions of local lines in Eq. (5) are not sufficient to match measured data. In particular, absorption data in the window ranges between spectral lines reflect a magnitude up to five times larger than predicted values. The excess is taken into account by a continuum spectrum N_c, which originates in the strong lines centered in the portion of the rotational H_2O spectrum that extends above 1 THz.[14, 20] Absolute absorption data from controlled experiments [15-19] provide the basis for formulating a physical model of N_c. Pure water vapor and foreign-gas (air, N_2) mixtures were studied at 18 - 40 GHz [15], 138 GHz [16], 186 - 194 GHz [17], 213.5 GHz [18], and 160 - 920 GHz [19].

At 137.8 GHz, pressure and temperature dependences of moist air absorption data were fitted with 10% rms to [16]

$$N_c'' = \nu\, e\,(k_s\, e + k_f\, p_d)10^{-7} \quad \text{ppm}, \qquad (6)$$

where $k_s = 3.57\,\theta^{7.5}$ and $k_f = 0.113\,\theta^3$. This equatiom was then applied to define the continuum for MPM89.[2]

At 213.5 GHz, new absorption data of moist nitrogen have been reported,[18] which fitted exceptionally well to Eq. (6):

$$k_s = 4.44\,\theta^{7.5} \text{ (0.4\% rms) and}$$

$$k_f = 0.145\,\theta^{4.5} \text{ (1.0\% rms).}$$

Analogous data closer to the 183-GHz line center [17] yielded initially a fitting error of 14.6% rms, which improved to 4.5% rms when the theoretical [12] strength value b_1 was increased by 5 percent. A theoretical approximation of the real part, [20]

$$N_c' = e\,\theta^{2.5}\, 0.791\times10^{-6}\,\nu^2 \quad \text{ppm},$$

was also considered in the fitting exercise. An analytical match of the continuum was considered by means of a *pseudo*-line centered out-of-band above 1 THz.

Expanding the line shape, Eq. (3), into a power series and assuming that $\delta = 0$, $\gamma_c \ll \nu_c$, and $\nu \to 0$, leads to:

$$N_c'' \approx 2\, S_c\, \gamma_c[(\nu/\nu_c) + 3\,(\nu/\nu_c)^3]\,/\,\nu_c^2 \quad \text{and}$$

$$N_c' \approx 2\, S_c\,[(\nu/\nu_c)^2 + (\nu/\nu_c)^4]\,/\,\nu_c \qquad (7)$$

Three different fits to Eq. (7) resulted in the following continuum line parameters:

ν_c	b_1	b_2	b_3	b_4	b_5	b_6	Data Ref.
GHz	kHz/mb		MHz/mb				
2200	4210	0.952	17.8	30.5	2.0	5.0	15, 18, 19
1780	**2230**	0.952	17.6	30.5	2.0	5.0	15, 18, Table 2
1470	1257	0.952	17.3	30.5	2.0	5.0	15, 18, 20

For the "continuum" line N_c centered at $\nu_c = 1780$ GHz and the chosen units one can assert that

$$k_s(\theta = 1) = 2\times10^4\, b_1\, b_3\, b_4 / \nu_c^3 = 4.34 \quad \text{GHz}^{-1}\,\text{mb}^{-2},$$

which is close to the value found by fitting the 213.5-GHz data alone (see above). The second-order ν-terms of Eq. (7) allow one to "tailor" the fit close to the upper frequency limit of MPM (1 THz) by changing ν_c. An exact fit to both measured absorption data [19] and analytical refraction results [20] around 900 GHz was not possible. Hence, the continuum line parameters ν_c and b_1 are a compromise which is of no consequence to data fits below about 800 GHz.

Table 2 lists the current line frequencies ν_ℓ and spectroscopic coefficients b_1 to b_6 (ν_ℓ and b_1 are from Ref. 12). Both the large widths for far-wing self-($b_3\times b_4$) and air-broadening (b_3) and the strong negative temperature dependence (b_6) have been suggested by theory.[14, 21] The b_1 values of the 22-GHz line* and 183-GHz [17] lines were increased by 5 percent to fit measured data.

The MPM93 for moist air is made up by $N = N_D + N_V$. Figures 2 to 4 give examples of MPM predictions for N'' in relationship to crucial published data. The critical temperature dependence of N_c'' is illustrated in Fig. 2. Frequency behavior of several data sets [15, 17-19] is shown in Figs. 3 and 4. The measured data [19] in Fig. 4 span a range from 160 to 920 GHz. Related attenuation rates $\alpha(\nu)$, including their continuum part, are shown in Fig. 5 for sea-level conditions (100%RH) at five temperatures (± 40°C).

2.4 Spectra of Water Droplets and Ice Particles

The interaction of suspended water droplets and ice crystals with radio waves is treated by employing the Rayleigh absorption approximation,

$$N_W = 1.5\,(w/m_{w,i})[(\epsilon_{w,i} - 1)/(\epsilon_{w,i} + 2)], \qquad (8)$$

where $m_{w,i} = 1$ and 0.916 (g/cm^3) are specific weights, and $\epsilon_{w,i}$ complex permittivities of water and ice, respectively.[4] For the size spectra ($r \leq 50\ \mu$m) of suspended water droplets, Eq. (8) is valid up to about 300 GHz. Fog or cloud conditions are specified by a mass density w. Water droplets form when the relative humidity exceeds saturation, u = 100-101 %, while t can be as low as -40°C (supercooled state). Propagation effects caused by suspended ice crystals (needles and plates) are primarily depolarizing and scattering in nature.

* The increase in the b_1-coefficient for the 22.2-GHz line was suggested by ground-level emission measurements.[13] Data at 20.6 GHz exhibited a systematic trend which was not apparent in 31.7 and 90 GHz data taken simultaneously. On-site radiosonde recordings of height profiles for p, t, and u furnished independent input to test three prediction models.

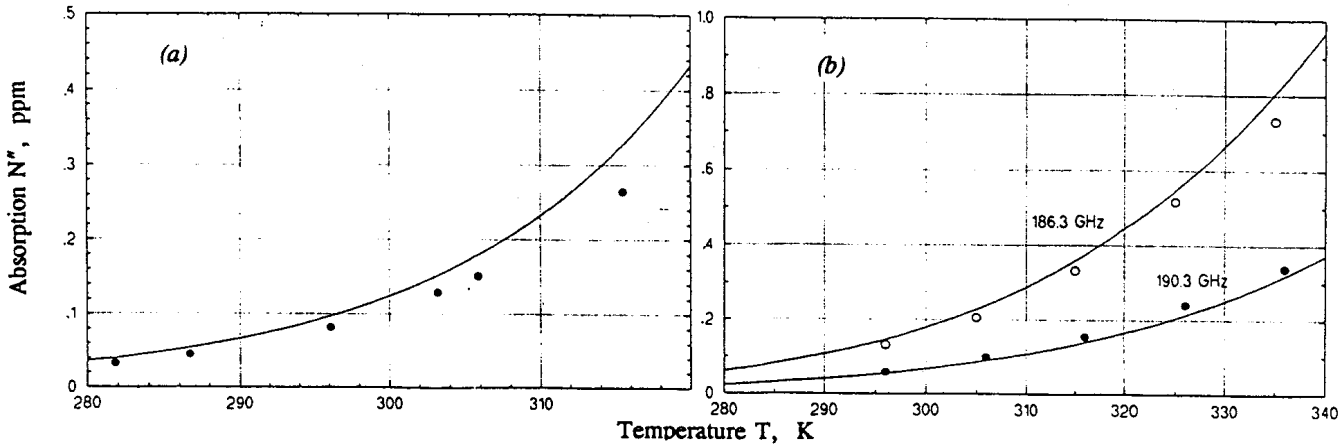

Figure 2. Absorption data N″ versus temperature T in kelvin: *(a)* moist air at 137.8 GHz (p = 1013 mb, u = 80%) [16], and *(b)* mixture of water vapor and nitrogen (186.3 and 190.3 GHz, p = 1000 mb, u = 10%) [17]. — MPM93.

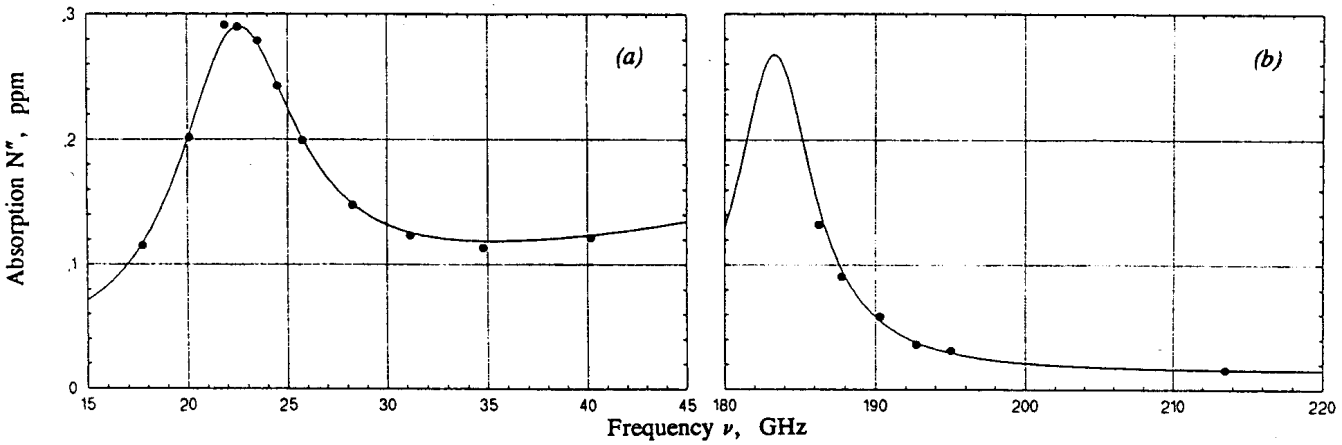

Figure 3. Absorption data N″ over two frequency ranges: *(a)* moist air (318 K, p = 1013 mb, u = 80%) [15], and *(b)* mixture of water vapor and nitrogen (296 K, p = 1000 mb, u = 10%) [17, 18]. — MPM93.

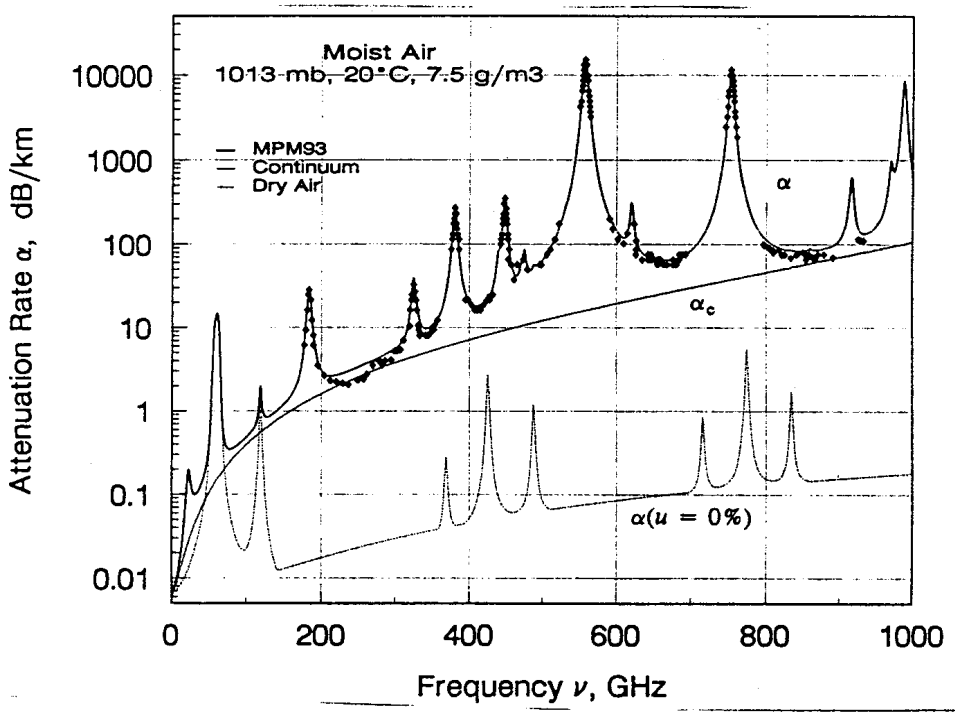

Figure 4. Attenuation rate α and continuum of moist air (u = 43.4%) and of dry air (u = 0) as predicted by MPM93 for standard sea-level conditions (p = 1013 mb, t = 20°C). Data points are from Ref. 19.

TABLE 1. Spectroscopic Coefficients of O_2 Lines in Air

Center Freq.	Strength		Width		Overlap	
ν_k	a_1	a_2	a_3*	a_4	a_5*	a_6*
GHz	kHz/mb		MHz/mb		10^3/mb	
50.474238	9.400E-08	9.694	0.89	0.8	0.240	0.790
50.987749	2.460E-07	8.694	0.91	0.8	0.220	0.780
51.503350	6.080E-07	7.744	0.94	0.8	0.197	0.774
52.021410	1.414E-06	6.844	0.97	0.8	0.166	0.764
52.542394	3.102E-06	6.004	0.99	0.8	0.136	0.751
53.066907	6.410E-06	5.224	1.02	0.8	0.131	0.714
53.595749	1.247E-05	4.484	1.05	0.8	0.230	0.584
54.130000	2.280E-05	3.814	1.07	0.8	0.335	0.431
54.671159	3.918E-05	3.194	1.10	0.8	0.374	0.305
55.221367	6.316E-05	2.624	1.13	0.8	0.258	0.339
55.783802	9.535E-05	2.119	1.17	0.8	-0.166	0.705
56.264775	5.489E-05	0.015	1.73	0.8	0.390	-0.113
56.363389	1.344E-04	1.660	1.20	0.8	-0.297	0.753
56.968206	1.763E-04	1.260	1.24	0.8	-0.416	0.742
57.612484	2.141E-04	0.915	1.28	0.8	-0.613	0.697
58.323877	2.386E-04	0.626	1.33	0.8	-0.205	0.051
58.446590	1.457E-04	0.084	1.52	0.8	0.748	-0.146
59.164207	2.404E-04	0.391	1.39	0.8	-0.722	0.266
59.590983	2.112E-04	0.212	1.43	0.8	0.765	-0.090
60.306061	2.124E-04	0.212	1.45	0.8	-0.705	0.081
60.434776	2.461E-04	0.391	1.36	0.8	0.697	-0.324
61.150560	2.504E-04	0.626	1.31	0.8	0.104	-0.067
61.800154	2.298E-04	0.915	1.27	0.8	0.570	-0.761
62.411215	1.933E-04	1.260	1.23	0.8	0.360	-0.777
62.486260	1.517E-04	0.083	1.54	0.8	-0.498	0.097
62.997977	1.503E-04	1.665	1.20	0.8	0.239	-0.768
63.568518	1.087E-04	2.115	1.17	0.8	0.108	-0.706
64.127767	7.335E-05	2.620	1.13	0.8	-0.311	-0.332
64.678903	4.635E-05	3.195	1.10	0.8	-0.421	-0.298
65.224071	2.748E-05	3.815	1.07	0.8	-0.375	-0.423
65.764772	1.530E-05	4.485	1.05	0.8	-0.267	-0.575
66.302091	8.009E-06	5.225	1.02	0.8	-0.168	-0.700
66.836830	3.946E-06	6.005	0.99	0.8	-0.169	-0.735
67.369598	1.832E-06	6.845	0.97	0.8	-0.200	-0.744
67.900867	8.010E-07	7.745	0.94	0.8	-0.228	-0.753
68.431005	3.300E-07	8.695	0.92	0.8	-0.240	-0.760
68.960311	1.280E-07	9.695	0.90	0.8	-0.250	-0.765
118.750343	9.450E-05	0.009	1.63	0.8	-0.036	0.009
368.498350	6.790E-06	0.049	1.92	0.2	0	0
424.763124	6.380E-05	0.044	1.93	0.2	0	0
487.249370	2.350E-05	0.049	1.92	0.2	0	0
715.393150	9.960E-06	0.145	1.81	0.2	0	0
773.839675	6.710E-05	0.130	1.82	0.2	0	0
834.145330	1.800E-05	0.147	1.81	0.2	0	0

TABLE 2. Spectroscopic Coefficients of H_2O Lines in Air

Center Freq.	Strength		Width			
ν_ℓ	b_1*	b_2	b_3	b_4	b_5	b_6
GHz	kHz/mb		MHz/mb			
22.235080	0.01130+	2.143	2.811	4.80	0.69	1.00
67.803960	0.00012	8.735	2.858	4.93	0.69	0.82
119.995940	0.00008	8.356	2.948	4.78	0.70	0.79
183.310091	0.24200+	0.668	3.050+	5.30	0.64	0.85
321.225644	0.00483	6.181	2.303	4.69	0.67	0.54
325.152919	0.14990	1.540	2.783	4.85	0.68	0.74
336.222601	0.00011	9.829	2.693	4.74	0.69	0.61
380.197372	1.15200	1.048	2.873	5.38	0.54+	0.89+
390.134508	0.00046	7.350	2.152	4.81	0.63	0.55
437.346667	0.00650	5.050	1.845	4.23	0.60	0.48
439.150812	0.09218	3.596	2.100	4.29	0.63	0.52
443.018295	0.01976	5.050	1.860	4.23	0.60	0.50
448.001075	1.03200	1.405	2.632	4.84	0.66	0.67
470.888947	0.03297	3.599	2.152	4.57	0.66	0.65
474.689127	0.12620	2.381	2.355	4.65	0.65	0.64
488.491133	0.02520	2.853	2.602	5.04	0.69	0.72
503.568532	0.00390	6.733	1.612	3.98	0.61	0.43
504.482692	0.00130	6.733	1.612	4.01	0.61	0.45
547.676440*	0.97010	0.114	2.600	4.50	0.70	1.00
552.020960*	1.47700	0.114	2.600	4.50	0.70	1.00
556.936002	48.74000	0.159	3.210	4.11	0.69	1.00
620.700807	0.50120	2.200	2.438	4.68	0.71	0.68
645.866155*	0.00713	8.580	1.800	4.00	0.60	0.50
658.005280	0.03022	7.820	3.210	4.14	0.69	1.00
752.033227	23.96000	0.396	3.060	4.09	0.68	0.84
841.053973	0.00140	8.180	1.590	5.76	0.33	0.45
859.962313	0.01472	7.989	3.060	4.09	0.68	0.84
899.306675	0.00605	7.917	2.985	4.53	0.68	0.90
902.616173	0.00426	8.432	2.865	5.10	0.70	0.95
906.207325	0.01876	5.111	2.408	4.70	0.70	0.53
916.171582	0.83410	1.442	2.670	4.78	0.70	0.78
923.118427*	0.00869	10.22	2.900	5.00	0.70	0.80
970.315022	0.89720	1.920	2.550	4.94	0.64	0.67
987.926764	13.21000	0.258	2.985	4.55	0.68	0.90
1780*	2230	0.952	17.6	30.5	2	5

*Different from MPM89 [2]
+Based on measured data

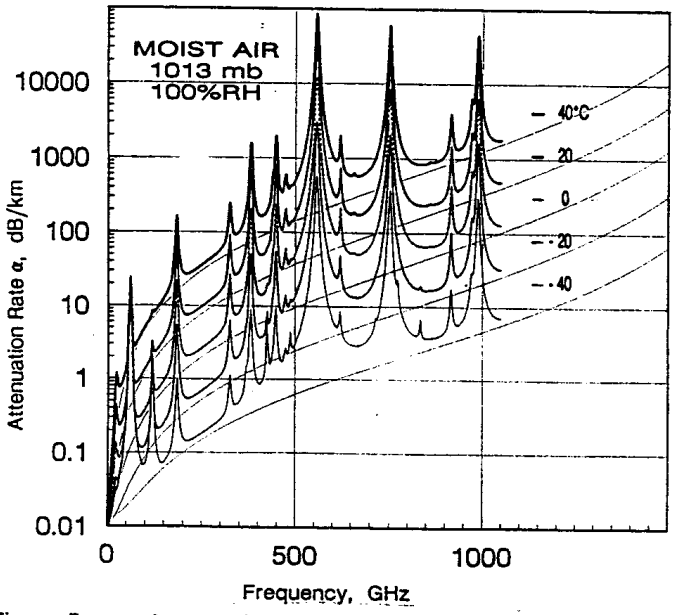

Figure 5. Attenuation α of moist air (u = 100%) for frequencies below 1000 GHz at sea-level (p = 1013 mb) and temperatures ± 40°C: —— MPM93, ···· Continuum.

Complex permittivity of pure water was expressed by a double-Debye model, [22]

$$\epsilon_w = \epsilon_o - \nu\,[(\epsilon_o - \epsilon_1)/(\nu + i\,\gamma_1) + (\epsilon_1 - \epsilon_2)/(\nu + i\,\gamma_2)], \quad (9)$$

which provided a best fit to measured ϵ_w data. The static and high-frequency permittivities are

$$\epsilon_o = 77.66 + 103.3\,(\theta - 1),$$

$$\epsilon_1 = 0.0671\,\epsilon_o, \qquad \epsilon_2 = 3.52;$$

and the two relaxation frequencies are

$$\gamma_1 = 20.20 - 146\,(\theta - 1) + 316\,(\theta - 1)^2,$$

$$\gamma_2 = 39.8\,\gamma_1 \quad \text{GHz}.$$

The slight temperature dependence of ϵ_2 (reported in Ref. 22) was eliminated to avoid nonphysical behavior for supercooled (-20 to -40°C) water at frequencies above 100 GHz.

A permittivity model for ice was reported by Hufford [23],

$$\epsilon_i = 3.15 + i\,(a_i/\nu + b_i\,\nu), \quad (10)$$

where

$$a_i = (\theta - 0.171)\exp(17.0 - 22.1\,\theta)$$

and

$$b_i = \{0.0542\,[\theta/(\theta - 0.993)]^2 + 6.33/\theta - 1.31\}10^{-5}.$$

The MPM93 for fog/cloud cases is $N = N_D + N_V + N_W$. Related attenuation (α) and delay (τ) rates up to 120 GHz are plotted in Fig. 6 for a normalized mass density, w = 1 g/m^3 (heavy fog, about 50 m visibility) deposited in saturated, sea-level air (± 30°C). Below freezing, liquid properties were changed to those of ice. Above freezing one notices that the combined attenuation is almost independent of temperature.

3. RADIO-PATH CHARACTERISTICS

The electromagnetic spectrum between 100 and 1000 GHz is available to expand radio services. This band offers favorable alternatives to both microwave and ir/optical systems. Applications in communication, radar, and remote sensing can profit from larger bandwidth, smaller antenna sizes for a given spatial resolution, high frequency resolution and, in contrast to ir/optical ranges, a favorable performance under fog/cloud conditions. Besides technical difficulties, the attenuating nature of the earth's atmosphere seriously limits usable path lengths. Except for a few window ranges, the medium at ground-levels ($h \leq 1$ km) is opaque due to strong absorption lines of water vapor. High mountain sites ($h \leq 4$ km), airplanes ($h \leq 15$ km), and balloons ($h \leq 35$ km) are alternative platforms to avoid these limitations.

A predictive broadband (1 - 1000 GHz) model for radio characteristics of the neutral atmosphere ($h \leq 130$ km) was developed to allow prompt evaluations of the highly variable propagation effects from basic data. Performance of established applications (≤ 30 GHz) can be translated to (frequency scaling) or combined with new schemes and economical assessments of feasible trade-offs and adaptive measures can be made.

3.1 Transmission and Emission Formulations

Propagation through the nonscattering and nonturbulent inhomogeneous atmosphere is described by the line integral $\int N\,ds$, where ds is a path differential and the refractivity N was discussed in Sect. 2. Height profiles of N are the basis for calculating delay and loss along the path. Excess delay,

$$D = 3.3356 \int (N_o + N')ds \quad \text{ps},$$

is linked to the real part and total path attenuation,

$$A = 0.1820\,\nu \int N''\,ds \quad \text{dB}, \quad (11)$$

to the imaginary part.[26] The transmission factor,

$$\Gamma = 10^{-0.1\,A}, \quad (12)$$

evaluates the energy transfer. A path is said to be opaque when less than 0.1% of the original energy is passed ($\Gamma \leq 0.001$, $A \geq 30$ dB). The absorbing atmosphere maintains, up to approximately 90 km height, thermal equilibrium and emits noise radiation at the equivalent blackbody temperature,

$$T_B = 4.191\cdot10^{-2}\,\nu \int T(s)\,N''(s)\,\Gamma(s_o,s)\,ds \quad \text{K}. \quad (13)$$

Decreasing transmission leads to increasing emission. The weighting function,

$$W(s) = 4.191\cdot10^{-2}\,\nu\,N''(s)\,\Gamma(s_o,s), \quad (14)$$

determines the height range from where the emission originates. Two cases can be made based on the integration limits for A. In the first one, A is evaluated "upwards", starting at the initial height, h_o; secondly, the start is at the final height, h_∞, and moves "downwards". Reciprocity between path attenuation A_i and brightness $T_{B,i}$ was assumed for polarization-sensitive computations based on the matrix $\mathbb{N}$.

3.2 Atmospheric Radio-Path Model

The MPM code (see Sect. 2) is applied in a radio-path model which simulates propagation through an inhomogeneous medium. The atmosphere is spherically stratified in concentric layers between h = 0 and 130 km separated by 1-km increments (Δh). Values for N(h) are enumerated by height profiles of p(h), t(h), and u(h). The U.S. Standard Atmosphere and the mid-latitude mean water-vapor profile [24] are the defaults of the path model. All computed examples given below are valid for the default case. It is not difficult to implement different model atmospheres or radiosonde data.

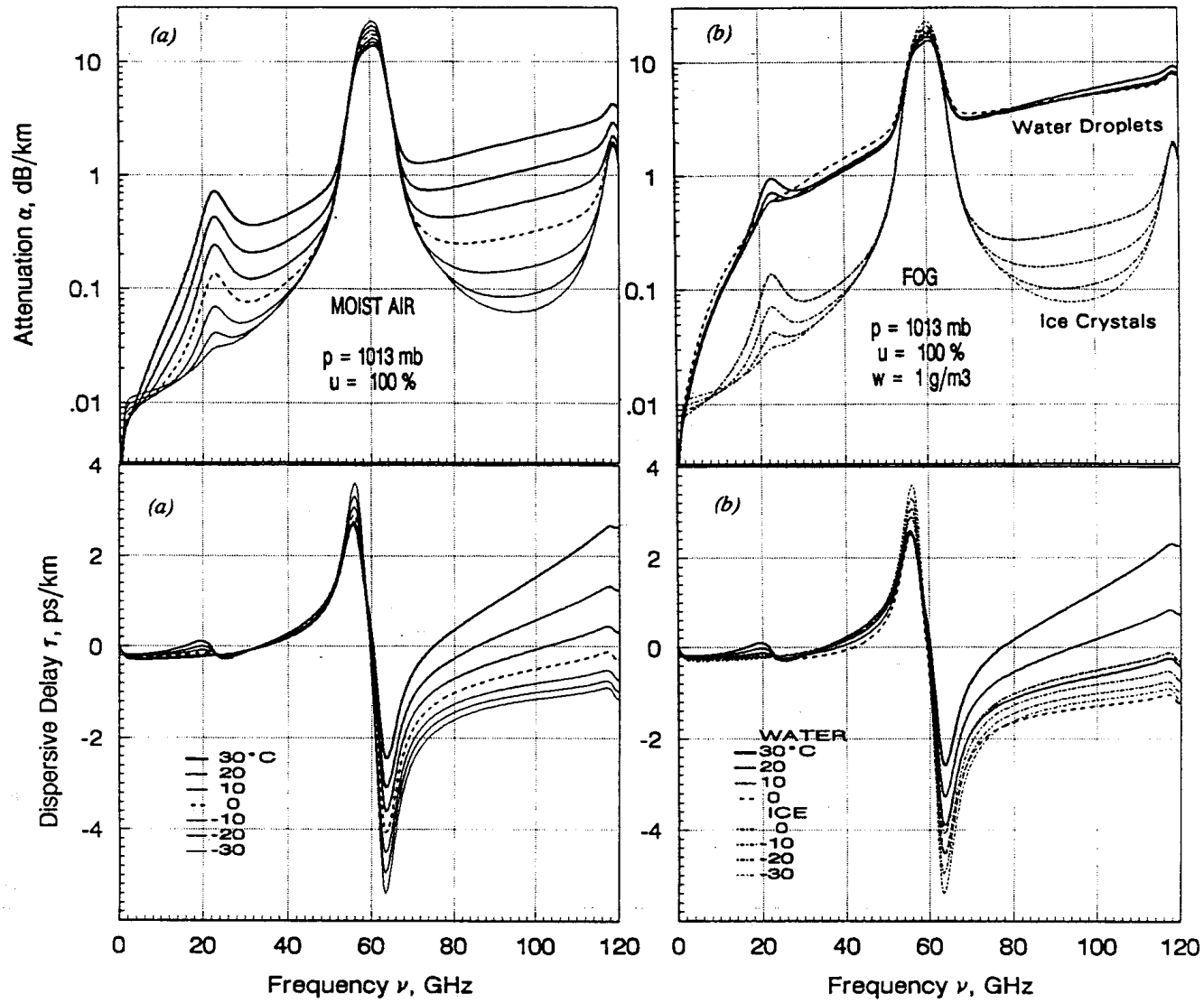

Figure 6. Attenuation rate $\alpha(\nu)$ and delay rate $\tau(\nu)$ up to 120 GHz at temperatures ± 30°C: *(a)* Moist air at sea-level, u = 100 %, *(b)* water droplets or ice crystals, w = 1 g/m^3, added to *(a)*.

The path differential ds of a slant path is computed by means of the rules of spherical geometry. For elevation angles, $\varphi \geq 10°$, the secant law $ds = \Delta h/\sin\varphi$ follows. Actually, both the curvature of the Earth and refraction determine the path extension of Δh. At very low elevation angles ($\varphi \to 0$), the height interval Δh is subdivided into 10×0.1-km and further, if needed, into 10×0.01-km groups to approximate more nearly a continuum of N values. When a maximum change of $A_h - A_{h-1} \geq 0.1$ dB is detected across an integration layer, the linear interpolation initiates automatically.

The numerical integration of A (Eq. 11) stops at heights h_∞ when increments ΔA become smaller than 0.01 dB (for a limb path after passing the tangential height). The path length L is that between h_o and h_∞. The numerical integration of T_B (Eq. 13) for emission radiating to the height level h_o follows

$$T_B \approx 0.2303 \sum_h [T(h)(A_h - A_{h-1})\,\Gamma(h)] + 2.7\,\Gamma(\infty), \quad (15)$$

where $2.7\,\Gamma(\infty)$ is the cosmic background term. Superfluous computations are stopped when $W(h) \leq 10^{-6}$. Results of the radio-path model are summarized for two frequencies, 21 and 45 GHz in Table 3. Listed are the path attenuation A of a ground-to-space link and the emission received at ground level. For $\varphi = 0$, the absorbing air mass at 21 GHz is 56 times the zenith value.

TABLE 3.
Total Attenuation A and Emission T_B at 21- and 45-GHz Through a Model Atmosphere.[24]

Surface values at h_o: 1013 mb, 15°C, q = 3.57 g/m^3
($V = \int q(h)dh$ = 10.6 mm for zenith, φ = 90°)

ν	A	T_B	φ	h_∞	L
GHz	dB	K	deg	km	km
21.0	0.28	19.2	90	11	11
	0.56	34.9	30	13	26
	0.82	48.5	20	15	44
	1.60	85.1	10	17	94
	15.7	274.4	0	26	577
45.0	0.66	39.2	90	17	17
	1.32	71.1	30	19	38
	1.93	96.4	20	22	64
	3.74	154.9	10	21	115
	32.0	285.6	0	31	650

3.3 Mesospheric Radio-Path Model

The intensity of O_2 microwave lines under mesospheric conditions ($\geq$ 40 km) is location-, direction-, and polarization-sensitive. Anisotropic transmission and emission effects must be recognized. Under these conditions the atmospheric path model program substitutes for N the refractivity matrix $\mathbb{N}$ ($\nu_k \pm 10$ MHz, Eq. 4), and becomes ZPM (Zeeman Propagation Model).[8,9] This routine requires numerous additional path parameters to perform a numerical integration of the path attenuation A_i :

- A ray is traced in geodetic coordinates marking altitude h above sea level, LA_titude and LO_ngitude [heights in N-S directions are adjusted to account for the flattening (1/298.25) of the earth]
- The wave direction is specified by AZ_imuth and elevation angle φ.
- A geomagnetic field model (MAGFIN [25]) computes magnitude and direction of the magnetic vector $\mathbf{B}^*$
- Polarization of launched wave or emitted noise power is selected (H/V-Linear or R/L-Circular)
- The frequency range is set in terms of deviation from a selected O_2 line center ($\Delta\nu = \nu_k \pm \nu$)

Two characteristic waves are represented by normalized Stokes parameters and combined to produce the initial polarization.[8] This combination is then traced through the propagation distance L. Eigenvalues and eigenvectors of the 2×2 plane-wave refractivity matrix for orientation angle ϕ between wave vector $\mathbf{E}^*$ and magnetic vector $\mathbf{B}^*$ are calculated. The propagating field is a linear combination of two characteristic waves.

Individual integration steps of ZPM are detailed in Table 4: A ray originates at the 300-km orbital height (h, LA, LO, AZ, and φ) and passes through the atmosphere to a minimum, tangential height, h_t = 90 km. The frequency is at line center (ν_k = 61.150 GHz). Complete attenuation spectra over the range, $\nu_k \pm 2$ MHz, are plotted in Fig. 7. Path attenuation A_i depends on the initial polarization (i ≡ HL, VL, RC, LC). The polarization selectivity of the Zeeman effect is evident when comparing it to the case B = 0.

3.4 Millimeter-Wave Limb Sounding

The Microwave Limb Sounder MLS on NASA's UARS satellite [26] and the Millimeter-wave Atmospheric Sounder MAS [27] on the space-shuttle (ATLAS Missions I, II, ...) both are very refined atmospheric spectrometers compared to instruments which simulate atmospheric conditions in the laboratory.[5] They measure geocoded thermal emission spectra of trace molecules up to altitudes of 150 km on a global scale. Profiles of molecular abundances, temperature, pressure, and magnetic field can be determined. Spectral signatures are recorded under most favorable conditions (i.e., 3 K background) and path lengths are thousand times longer than available for laboratory work. Unheard-of detection sensitivities bring answers to old problems and raise many new questions. Here one measurement example from MAS is presented to serve as a test case for ZPM predictions.

MAS consist of three multi-channel radiometers, tuned to detect emission from O_2 (61.1, 63.0, 63.6 GHz), H_2O (183 GHz), and the trace gases O_3 (184 GHz) and ClO (204 GHz). The antenna (beamwidth 0.3° at 61 - 64 GHz; polarized HL) is scanned downwards from a 300-km orbit level through the limb. Typically, the continuous vertical scan repeats every 12.8 seconds. Each scan is calibrated (2.7 and 300 K) and geocoded. The radiometers are superheterodyne receiver with double-sideband (DSB) detection. A filter bank follows, which separates the received noise into 10× 40-MHz, 20× 2-MHz, and 20× 0.2-MHz spectral channels.

From one partial orbit, the emission data of three O_2 lines centered at 61.15-, 63.00-, and 63.57 GHz were analyzed for tangent heights ranging from 125- to 12 km at the most northern point (shuttle at 57°N, antenna looks north) and at the equator.[28] The calibrated data were available in 5-km height steps, each averaged over five scans (1.2 s integration time). The specific example to be reviewed here was recorded in a lower sideband range centered at ν = 61.150 GHz (O_2 line center), while the upper sideband (image) at 71.630 GHz received cosmic background radiation (2.7 K). To first order, the recorded mean is about half the theoretical single sideband signal.

TABLE 4.

Path Attenuation $A_i(h)$ and Noise Emission $T_{B,i}$ for a Limb Path (h_t = 90 km) at ν_o = 61.15056 GHz. Antenna is located at 57°N/70°W, h = 300 km and looks down (φ = -14.57°) towards north (AZ = 0°) to receive linear-polarized radiation (results for i = VL-, RC- and LC-polarizations are also given).

h	LA	LO	AZ	φ	B	ϕ	L	A_{HL}	A_{VL}	W_{HL}	W_{VL}	A_{RC}	A_{LC}
km	deg	deg	deg	deg	μT	deg	km	dB		km^{-1}		dB	
300	**57.0**	**-70**	**0**	**-14.57**			0	T_B(DBS) = **67.8** K (ZPM)				63±2 K (MAS)	
↓							↓	T_B(SSB) =		131.2	174.5	153.0	153.0 K
129	65.2	-70	0	-6.39	55.1	78.4	954	0.00	0.00	.000	.000	0.00	0.00
↓							↓			↑			
91	70.4	-70	0	-1.14	55.4	85.6	1548	1.30	2.92	.060	.094	2.03	2.03
90	71.0	-70	0	**-0.53**	55.4	86.2	1616	1.97	4.45	**.099**	.126	3.04	3.04
91	72.1	-70	0	**0.53**	55.3	87.3	1736	3.39	7.66	**.150**	.127	5.02	5.02
92	72.7	-70	0	1.14	55.2	88.4	1805	4.06	9.20	.061	.042	5.91	5.91
↓							↓						
129	77.7	-70	0	6.15	53.7	94.9	2371	5.15	11.68	.000	.000	7.29	7.29
130	77.8	-70	0	6.23	53.7	95.0	2380	**5.15**	11.68	.000	.000	7.29	7.29

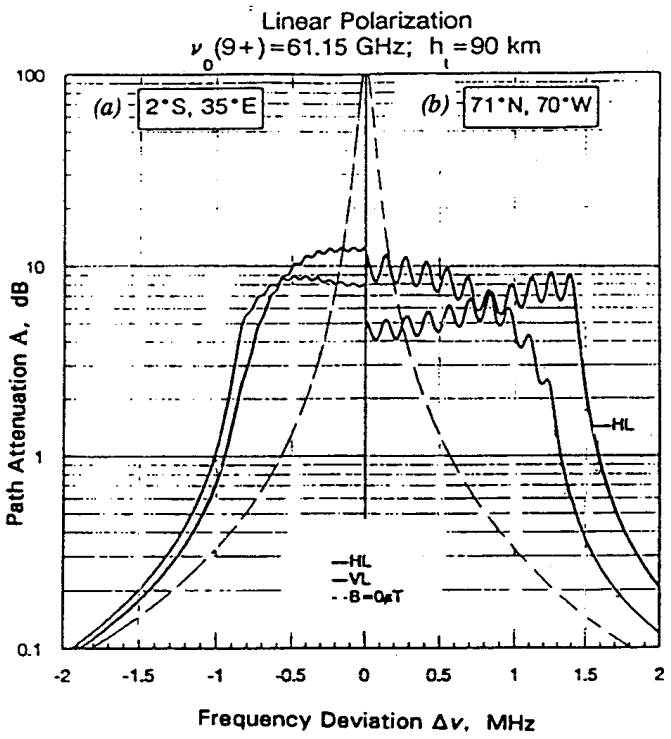

Figure 7. Spectra (ν_0 ± 2 MHz) of total attenuations A_i (i = HL, VL) and A_0 (B = 0) for a limb path (h_t = 90km) through the U.S. Std. Atm.[24] at two locations marked (a) and (b).

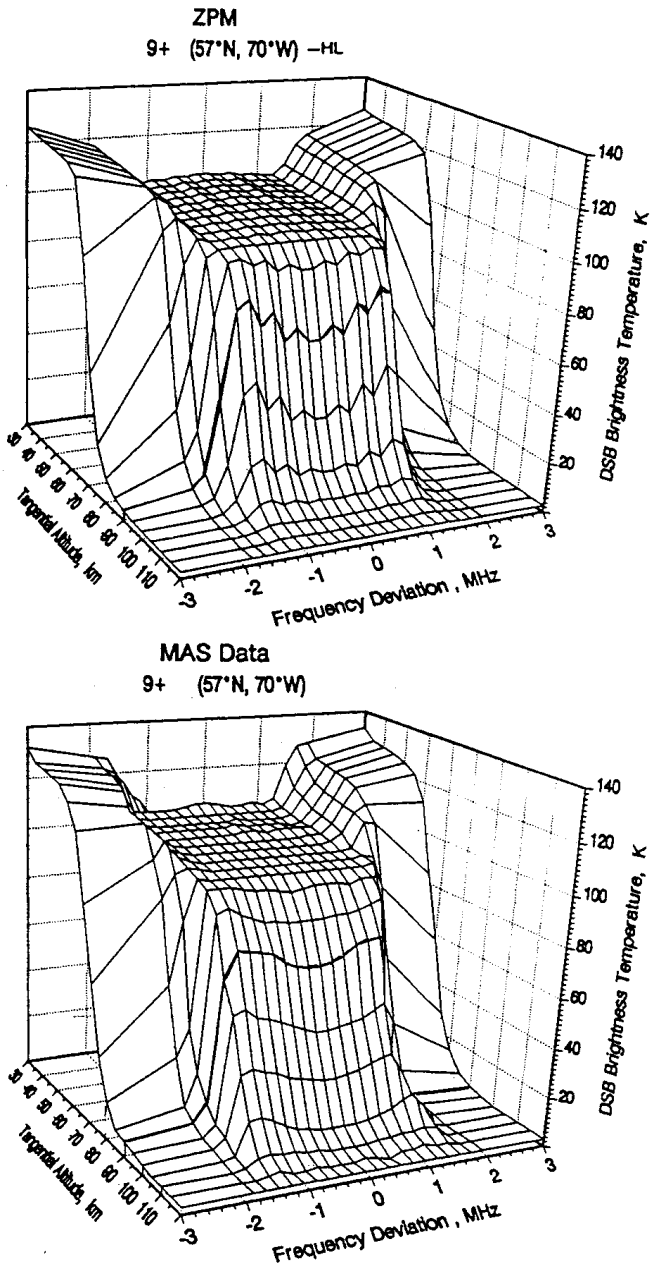

Figure 8. DSB-emission of the 9+ line (ν_k ± 3 MHz) from a limb scan, h_t = 30 to 120 km, approximatly centered over 70°N, 70°W: *(a)* ZPM predictions for HL polarization and *(b)* MAS data**.

Results of ZPM simulations and actually measured 396 data points are depicted in Fig. 8. The predictions reproduced the experimental scenario from basic knowledge of the MAS spectrometer operation and standard atmospheric models.[24,25] Limb-emission received by MAS from tangential heights ranging from 30 to 120 km at a northern location (71°N/70°W) is consistent with ZPM predictions. The path variables that were required to compute a value of T_B are listed in Table 4 for the case at center frequency ν_k. The weighting function W(h), Eq. (14) indicates very height-selective ($\Delta h \leq 1$ km) temperature sounding between 110 and 80 km. At h_t = 78 km the path becomes abruptly opaque and T_B assumes about half the physical temperature of the 78-km level (98 K). Below h_t = 35 km, the upper sideband "warms up" due to continuum absorption by water vapor and air at 71.63 GHz (MPM), which raises the value for $T_B(\nu_k)$. A switchable filter to isolate the upper sideband channel could be used to look at 71.6 GHz all the way down to ground levels.

4. CONCLUSIONS

Propagation characteristics of the atmosphere are predicted by the general refractivity N, and for Zeeman-broadening by the special refractivity matrix $\mathbb{N}$. Transmission and emission properties of the inhomogeneous atmosphere (e.g., excess path delay, total attenuation, opacity, sky noise, etc.) were modeled from known path profiles of physical variables.

MPM93 reproduces the spectral characteristics of the clear atmosphere (O_2, H_2O) between 18 and 930 GHz within the uncertainty limits of a restricted number of controlled experiments that have been reported.[15 - 19]

ZPM reproduces the main features of measured thermal radiation signatures of a Zeeman-split oxygen line as a solution to the forward-transfer problem[8, 9, 28] and can serve as a starting point to develop profile inversion algorithms.[7, 13] Validation, error checking of predictions, and incorporation of new research results will continue to be critical and time consuming tasks in the effort to refine understanding and modeling of electromagnetic wave propagation through the neutral atmosphere.

** The MAS-project was supported by the German agencies BMFT and DARA under FKZ 50 QS 8502, 9002, by NASA, and by the MAS-PI agencies: MPAE (Katlenburg-Lindau, FRG); NRL (Washington, D.C., USA); IAP (Berne, CH); and IFe (Bremen, FRG).

ACKNOWLEDGMENTS
The work was supported in part by the U. S. Army Atmospheric Sciences Laboratory, ARL, SLCAS-BA under Reference No. ASL 92-8058.

5. REFERENCES

1. Liebe, H.J.,"An Updated Model for Millimeter Wave Propagation in Moist Air," Radio Sci., *20*, 5, May 1985, pp 1069-1089.

2. Liebe, H.J.,"MPM - An Atmospheric Millimeter-Wave Propagation Model", Int. J. Infrared and Millimeter Waves, *10*, 6, July 1989, pp 631-650.

3. Rosenkranz, P.W.,"Absorption of Microwaves by Atmospheric Gases", in "Atmospheric Remote Sensing By Microwave Radiometry"; Janssen, M.A., ed.; J. Wiley & Sons, Inc., 1993 (ISBN 0 471 62891 3), pp 37-90.

4. Liebe, H.J., Manabe, T. and Hufford, G.A.,"Millimeter-Wave Attenuation and Delay Rates Due to Fog/Cloud Conditions", IEEE Trans. Antennas Propag., *AP-37*, 12, December 1989, pp 1617-1623.

5. Liebe, H.J., Rosenkranz, P.W. and Hufford, G.A.,"Atmospheric 60-GHz Oxygen Spectrum: New Measurements and Line Parameters", J. Quant. Spectr. Radiat. Transf., *48*, 5, Nov./Dec. 1992, pp 629-643.

6. Crawford, A.B. and Hogg, D.C.,"Measurement of Atmospheric Attenuation at Millimeter Wavelengths", Bell Syst. Techn. J., *35*, 7, July 1956, pp. 907-916.

7. Rosenkranz P.W. and Staelin, D.H.,"Polarized Thermal Emission from Oxygen in the Mesosphere", Radio Sci., *23*, 5, May 1988, pp 721-729.

8. Hufford G.A. and Liebe, H.J.,"Millimeter-Wave Propagation In The Mesosphere", NTIA-Report *89-249*, U.S. Dept. Commerce, Boulder, CO, 1989; NTIS Order No. PB 90-119868/AF (1989).

9. Liebe, H.J. and Hufford, G.A.," Modeling Millimeter-wave Propagation Effects in the Atmosphere", AGARD *CP-454*, October 1989, Paper 18.

10. Goff, J.A. and Gratch, S.,"Low-Pressure Properties of Water from -160 to 212°F", Trans. Amer. Soc. Heat. Vent. Eng., *52*, 1946, pp 95-121 (also see List, R.J., "Smithonian Meteorological Tables", Washington D.C., Smithonian Inst., 1966).

11. Bauer, A., Godon, M., Kheddar, M. and Hartmann, J.M., "Temperature and Perturber Dependences of Water Vapor Line-Broadening: Experiments at 183 GHz, Calculations Below 1000 GHz", J. Quant. Spectr. Radiat. Transf., *41*, 1, 1989, pp 49-54.

12. Poynter, R.L., Pickett, H.M., and Cohen, E.,"Submillimeter, Millimeter, and Microwave Spectral Line Catalogue", JPL Publication 80-23, Revision 3, 1991, NASA-JPL, Pasadena, CA.

13. Westwater, Ed.R.,"Groundbased Microw. Radiometry ", in "Atmospheric Remote Sensing By Microwave Radiometry", Janssen, M.A., ed.; J. Wiley & Sons, Inc., 1993 (ISBN 0 4710 62891 3), pp 145-213.

14. Ma, Q. and Tipping, R.H.,"Water Vapor Continuum in the Millimeter Spectral Region ", J. Chem. Phys., *93*, 9, Sept. 1990, pp 6127-6139.

15. Becker, G.E. and Autler, S.H.,"Water Vapor Absorption of Electromagnetic Radiation in the Centimeter Wavelength Range", Phys. Rev., *70*, 1946, pp 300-307.

16. Liebe, H.J.," A Contribution to Modeling Atmospheric Millimeter-Wave Properties", Frequenz, *41*, 1/2, Jan./Feb. 1987, pp 31-36.

17. Bauer, A. and Godon, M.,"Temperature Dependence of Water Vapour Absorption in Line-Wings at 190 GHz", J. Quant. Spectr. Rad. Transf., *46*, 3, 1991, pp 211-220.

18. Godon, M., Carlier, J. and Bauer, A.,"Laboratory Studies of Water Vapor Absorption in the Atmospheric Window at 213 GHz", J. Quant. Spectr. Radiat. Transf., *47*, 4, 1992, pp 275-285.

19. Furashov, N.I., Katkov, V.Yu. and Svertlov, B.A., "Submillimetre Spectrum of the Atmospheric Water Vapor Absorption- Some Experimental Results", ICAP 89, IEE Conf. Publ., No. *301*, 1989, pp 310-311.

20. Hill, R.J.,"Dispersion by Atmospheric Water Vapor at Frequencies Less Than 1 THz", IEEE Trans. Antennas Propag., *AP-36*, 3, March 1988, pp 423-430.

21. Rosenkranz, P.W.,"Pressure Broadening of Rotational Bands.II. Water Vapor from 300 to 1100 cm^{-1} ", J. Chem. Phys., *87*, 7, July 1987, pp 163-170.

22. Liebe, H.J., Hufford, G.A. and Manabe, T.,"A Model for the Complex Permittivity of Water at Frequencies Below 1 THz", Int. J. Infrared and Millimeter Waves, *12*, 7, July 1991, pp 659-675.

23. Hufford, G.A.,"A Model for the Complex Permittivity of Ice at Frequencies Below 1 THz", Int. J. Infrared and Millimeter Waves, *12*, 7, July 1991, pp 677-680.

24. COESA, U.S. Committee on Extension to the Standard Atmosphere,"U.S. Standard Atmosphere 76", NOAA-S/T *76-1562*; U.S. Gov. Printing Office, Washington, D.C., 1976.

25. Barraclough, D.R.,"International Geomagnetic Reference Field revision 1985", Pure and Appl. Geophys., *123*, 1985, pp 641-645.

26. Waters, J.W.,"Submillimeter-Wavelength Heterodyne Spectroscopy and Remote Sensing of the Upper Atmosphere", Proc. IEEE, *80*, 11, November 1992, pp 1679-1701.

27. Croskey, C.L. et al., "The Millimeter Wave Atmospheric Sounder (MAS): A Shuttle-Based Remote Sensing Experiment", IEEE Trans. Microw. Theory and Techniques, *MTT-40*, 6, June 1992, pp 1090-1099.

28. Cotton, M.A., Degenhardt, W., Hartmann, G.K., Hufford, G.A., Liebe, H.J., and Zwick, R.,"Analysis of MAS Emission Signatures from three O_2 Microwave Lines", NTIA Report 93-000, in preparation, 1993.